TSPO-PET and diffusion-weighted MRI for imaging a mouse model of infiltrative human glioma Running title: Imaging glioma infiltration

Hayet Pigeon, Elodie A. Pérès, Charles Truillet, Benoît Jego, Fawzi Boumezbeur, Fabien Caillé, Bastian Zinnhardt, Andreas H Jacobs, Denis Le Bihan, Alexandra Winkeler

TSPO-PET and diffusion-weighted MRI for imaging a mouse model of infiltrative human glioma

Running title: Imaging glioma infiltration

Hayet Pigeon, Elodie A. Pérès, Charles Truillet, Benoit Jego, Fawzi Boumezbeur, Fabien Caillé, Bastian Zinnhardt, Andreas H. Jacobs, Denis Le Bihan, Alexandra Winkeler

UMR 1023, IMIV, Service Hospitalier Frédéric Joliot, CEA, Inserm, Univsité Paris Sud, CNRS, Université Paris-Saclay, Orsay, France (H.P., C.T., B.J., F.C., A.W.) ; NeuroSpin, CEA/Université Paris-Saclay, Gif sur Yvette, France (E.A.P., F.B., D.LB.) ; Normandie Univ, UNICAEN, CEA, CNRS, ISTCT/CERVOxy group, Caen, France (E.A.P.) ; EIMI & Department of Nuclear Medicine, University Hospital Münster, Westfälische Wilhelms University Münster, Germany (B.Z., A.H.J.) ;Department of Geriatrics, Johanniter Hospital, Evangelische Kliniken, Bonn, Germany (A.H.J.)

*** Correspondence**: Alexandra Winkeler, PhD

CEA - Service Hospitalier Frédéric Joliot

4, place du Général Leclerc

F-91401 ORSAY Cedex

Tel. +33 1 69 86 7801

Fax. +33 1 69 86 7786

alexandra.winkeler@cea.fr

Funding

This work was performed on a platform of France Life Imaging network partly funded by the grant "ANR-11-INBS-0006"and the EU 7th Framework Programme (FP7/2007-2013) under grant agreement n° 278850 (INMiND).

Conflict of interest

The authors report no conflicting interests.

Authorship

Conception and design: HP, EAP, AW

Methodology development: HP, BJ, DLB, AW

Data acquisition: HP, EAP, BJ, CT, FC, AW

Data analysis/interpretation: HP, EAP, CT, FB, BZ, AHJ, DLB, AW

Manuscript writing, review, revision: HP, EAP, CT, FB, FC, BZ, AHJ, AW

Radiotracer production and quality: FC

5998 words

Abstract

Background

Glioblastoma is the most devastating brain tumor. Despite the use of multimodal treatments, most patients relapse, often due to the highly invasive nature of gliomas. However, the detection of glioma infiltration remains challenging. The aim of this study was to assess advanced positron emission tomography (PET) and magnetic resonance imaging (MRI) techniques for visualizing biological activity and infiltration of the tumor.

Methods

Using multi-modality imaging, we investigated [18F]DPA-714, a radiotracer targeting the 18kDa translocator protein (TSPO), [18F]FET PET, non-Gaussian diffusion MRI (ADC_0, Kurtosis), and the S-index, a composite diffusion metric, to detect tumor infiltration in a human invasive glioma model. *In vivo* imaging findings were confirmed by autoradiography and immunofluorescence.

Results

Increased tumor-to-contralateral [18F]DPA-714 uptake ratios (1.49 ± 0.11) were found starting 7 weeks after glioma cell implantation. TSPO-PET allowed visualization of glioma infiltration into the contralateral hemisphere two weeks earlier compared to the clinically relevant biomarker for biological glioma activity [18F]FET. Diffusion-weighted MRI (DWI), in particular kurtosis was more sensitive than standard T2w MRI to detect differences between the glioma-bearing and the contralateral hemisphere at 5 weeks. Immunofluorescence data reflect *in vivo* findings. Interestingly, labelling for tumoral and stromal TSPO indicates a predominant expression of TSPO by tumor cells.

Conclusion

These results suggest that advanced PET and MR imaging methods, such as [18F]DPA-714 and DWI, may be superior to standard imaging methods to visualize glioma growth and infiltration at an early stage.

Keywords: *[^{18}F]DPA-714, TSPO, glioma, diffusion MRI,* S-index

Key Points:

- *Longitudinal TSPO-PET and diffusion MRI of a mouse model monitor infiltrative human glioma*
- *Early glioma detection with [^{18}F]DPA-714 as compared to the clinical PET biomarker [18F]FET*

Importance of the study

Invasiveness of glioma cells into the brain parenchyma is a major issue for failure of glioblastoma treatment and tumor recurrence. However, common non-invasive imaging techniques fail to monitor these invading cells. Here, we report the use of TSPO-PET and DWI to follow tumor growth and invasion into the brain parenchyma using an invasively growing human glioblastoma model. TSPO-PET imaging accurately reflects GBM infiltration into the contralateral brain hemisphere, whereas diffusion kurtosis imaging detects early differences between the tumor and the contralateral brain parenchyma. This multi-modality approach to monitor GBM invasiveness will improve the early detection of glioma invasion, help to assess therapy response and will be readily available for clinical translation.

Introduction

Glioblastoma (GBM) is the most common and aggressive form of primary human brain tumors. Although GBM therapy consists of aggressive multimodal treatments including surgery, radiation and concomitant and adjuvant chemotherapy, the currently available treatment options have limited efficacy[1]. Invasion of glioma cells into the surrounding brain parenchyma is a hallmark of GBM and one of the reasons for treatment failure[2,3]. Imaging glioma cell infiltration remains challenging but advanced magnetic resonance imaging (MRI) and positron emission tomography (PET) might help in visualizing directly or indirectly the growth of diffuse glioblastomas[4].

Diffusion-weighted MRI (DWI) probes tissue at a microscopic scale, well below image resolution, by measuring the interaction of diffusing water molecules with tissue elements. Hence, DWI reveals unique information about brain microarchitecture[5]. By modeling the signal attenuation (S/S_0) using a non-Gaussian diffusion model[6], parametric maps can be computed for the apparent diffusion coefficient (ADC_0) and kurtosis (K). These non-Gaussian diffusion parameters can help distinguishing malignant from benign lesions in a rat brain tumor model[7]. Clinical studies have demonstrated that DWI parameters are helpful for grading gliomas by measuring the increased heterogeneity in more malignant tumors[8] and could be relevant as predictive biomarker of patient's outcome after treatment[9,10]. Consistently, recent studies suggested the use of DWI to characterize tumor infiltration[11] and improve delineation of the tumor margin[12]. A novel composite diffusion metric, designed as signature index (S-index*)* was proposed to distinguish tumoral from normal tissue. The S-index combines perfusion and diffusion parameters to enhance the sensitivity of DWI to assess tumor function and heterogeneity[13].

Moreover, PET as a molecular imaging technique has been suggested as promising alternative in glioma imaging, in particular for tumor growth and delineation of the tumor border[14]. Recent preclinical imaging studies suggested PET imaging of the translocator protein of 18kDa (TSPO) as a potential molecular imaging technique to improve tumor detection and possibly track glioma cell infiltration[15,16].

Initial studies on TSPO and TSPO ligands in the brain indicated that the density of TSPO was high in malignant gliomas and glioma cell lines, but low in normal/unaffected brain tissue[17,18]. Furthermore, TSPO expression levels positively correlated with the grade of malignancy and showed a negative correlation between TSPO expression and survival[19,20]. Some results also propose TSPO as a marker of glioma invasiveness[21,22]. TSPO expression can be monitored non-invasively using radiolabeled TSPO ligands. Several classes of TSPO radioligands have been developed in the last two decades, including the second generation TSPO tracer, N,N-diethyl-2-(2-(4-(2-[^{18}F]fluoroethoxy)phenyl)-5,7-dimethylpyrazolo[1,5-a]pyrimidin-3-yl)acetamide ([^{18}F]DPA-714). We and others have shown specific [^{18}F]DPA-714 imaging in different models of rat glioma[23-25]. Lately, a preclinical PET imaging study using another TSPO radioligand N-(2,5-dimethoxybenzyl)-2-[^{18}F]-fluoro-N-(2-phenoxyphenyl)acetamide ([^{18}F]PBR06) demonstrated elevated tracer uptake in human glioma xenotransplants according to the tumor grade and indicated infiltrative glioma growth not visible on conventional MR imaging[26].

We investigated the potential of TSPO-PET and diffusion-weighted MRI to assess glioma cell infiltration. Infiltrative glioma growth was monitored longitudinally alone and in combination with conventional T_2-weighted imaging (T_2w) and DWI in a human invasively growing glioma model. We hypothesized that [^{18}F]DPA-714 PET and DWI, in particular the composite S-index, can be used i) to track glioma infiltration into the surrounding brain parenchyma and ii) to monitor glioma growth earlier than with T_2w MRI or the clinically established PET-marker for endothelial amino acid transport O-(2-^{18}F-fluoroethyl)-L-tyrosine ([^{18}F]FET)[27].

Material and Methods

Study design & animal model

Longitudinal PET and combined PET/MRI studies were conducted to investigate the sensitivity and specificity of TSPO-PET as well as DWI to image infiltrative glioma growth. Animal studies were approved by the animal ethics committee of local authorities and were conducted in accordance with the ARRIVE guidelines and Directives of the European Union on animal ethics and welfare. Male NMRI nu/nu mice (Janvier Labs), 5-7 weeks old were housed in standard conditions under a regular 12h-dark/light cycle. Food and water were available *ad libitum*.

2 x 10^5 human glioblastoma cells in 1 µL Neurobasal medium were stereotactically implanted in the right striatum (2.5mm lateral to the bregma and 3 mm deep) of NMRI nu/nu mice. In total, 27 mice were orthotopically implanted with human P3 cells and imaged at week 1, 3, 5, 7 and 9 post cell implantation (p.i.), respectively. A more detailed description is given in supplementary Figure S1. At the end of the last PET scan, mice were euthanized, brains removed and frozen immediately in for histology and autoradiography.

Cell culture

The P3 human glioblastoma cells used in the present study, obtained from Pr. Hrvoje Miletic (Department of Biomedicine - Translational Cancer Research, University of Bergen, Norway), were derived from one GBM patient (P3) and have previously been characterized in a human GBM-derived xenograft model in nude rats[28]. Glioma cells displayed typical growth patterns and phenotypes *in vitro* and *in vivo*. The cells were not further genetically authenticated. Cells were grown in Neurobasal Medium containing x1 GlutaMax, x1 B27 supplement, 20 ng/mL bFGF and EGF, x1 penicillin/streptomycin (all from Gibco, Life Technologies) and 32 U/mL heparin (Panpharma) at 37°C in a 5% CO_2/95% air atmosphere.

Radiochemistry

[^{18}F]DPA-714 and [^{18}F]FET were synthesized as previously described[29,30]. [^{18}F]DPA-714 was obtained in 28 ± 5%, [^{18}F]FET in 44 ± 7% decay corrected radiochemical yield with radiochemical purity above 99% and molar activity of 158 ± 68 GBq/µmol and and 150 ± 51 GBq/µmol, respectively.

PET acquisitions

During all experimental procedures mice were anesthetized with isoflurane (3.0% for induction, 1.5 - 2% for maintenance of anesthesia) in 100% O_2. PET images were acquired on a Siemens Inveon® small animal PET or PET-CT scanner. Both scanners were used in parallel in order to assure a high specific radioactivity at the time of injection. Static PET scans of were acquired 30-60 minutes after a tail vein injection of 8.2 ± 3.6 MBq [^{18}F]DPA-714 or 7.2 ± 0.6 MBq [^{18}F]FET. For attenuation correction a CT or a transmission scan using an external 68Ge point source was performed. Images were reconstructed using Fourier rebinning (FORE) and a 2D ordered subset expectation maximization (OSEM) algorithm (16 subsets and 4 iterations). Except for the first time point (5 weeks p.i.), PET image acquisition was performed within 24h after MRI acquisition.

MRI acquisitions

MRI experiments were conducted on a 11.7 T Biospec MR scanner equipped with a CryoProbe dedicated for mouse brain imaging (Bruker BioSpin) as previously described[31]. For more details see supplementary data.

Data analysis

PET image analysis was performed using VINCI (Version: 4.63.0; http://www.nf.mpg.de/vinci3/) a graphical image analysis package equipped with image co-registration tools[32]. For quantitative analysis a volume-of-interest (VOI) analysis was performed on the summed image data sets (30-60 min). Three VOIs were manually delineated, one around the tumor-injection site in the ipsilateral hemisphere (T),

one in the contralateral striatum (C) and one on the corpus callosum (CC). Ipsi-to-contralateral and ipsilateral-to-corpus-callosum ratios as well as standardized uptake values (SUVs) were calculated. The SUV is defined as tissue radioactivity concentration in kBq/mL / ((injected dose in kBq) / (bodyweight in g)).

For image co-registration [^{18}F]DPA-714 PET-CT images were manually co-registered to the corresponding T_2w MRI and [^{18}F]FET PET-CT images, respectively, using the contour and image co-registration tool of VINCI. A thresholding approach was applied on [^{18}F]DPA-714 PET images as previously described[16], and detailed in supplementary data.

DWI data were processed using a home-made software implemented with MATLAB (Mathworks) and as previously described[31]. Details can be found in supplementary data. For each animal, a region-of-interest corresponding to the brain tumor (ipsilateral ROI) was manually delimited in the striatum on three consecutive slices, identified from the presence of tumor cell injection site. For this ispilateral ROI, the cell injection site identified by T2-hyposignal was excluded to avoid biasing the results. In the striatum of the hemisphere opposite to the tumor injection site, a contralateral ROI was delimited on the same slices. Mean values for ADC_0, kurtosis and S-index for each ROI were calculated.

Autoradiography, histology and immunohistochemistry

Frozen brain sections (20-µm thick) of whole tumor specimen were cut using a cryostat (Leica). Immunohistochemistry, autoradiography and hematoxylin/eosin staining were performed on adjacent 20-µm thick brain sections as previously described[33] or according to the manufacturer's instructions (Labonord). For more details, see supplementary data.

Statistical analysis

All data are presented as mean ± standard deviation. The statistical analyses were performed using GraphPad Prism software, version 6.05 (Graph Pad software Inc.). Comparisons of PET and DWI data between ipsilateral and contralateral VOI over time were performed using a one-way ANOVA and

Bonferroni multiple comparison tests for post hoc analysis. Differences in radiotracer uptake ratios ([^{18}F]DPA-714, [^{18}F]FET) were tested using a *t*-test. Significance levels were set at $p<0.05$.

Results

Longitudinal [^{18}F]DPA-714 PET images of human invasive glioma

PET imaging using the TSPO radioligand [^{18}F]DPA-714 shows an increase in [^{18}F]DPA-714 uptake in the ipsilateral (tumor-bearing) brain hemisphere over time. From 7 weeks p.i. onwards extended [^{18}F]DPA-714 uptake in the ipsilateral hemisphere was observed. [^{18}F]DPA-714 highlights infiltration of the tumor into the contralateral hemisphere via the corpus callosum (CC) after 7-9 weeks of glioma growth (Fig. 1 A, C). The mean SUVs after one (0.22 ± 0.06 vs 0.18 ± 0.04; n=10), three (0.19 ± 0.06 vs 0.17 ± 0.06; n=9) or five (0.28 ± 0.11 vs 0.23 ± 0.10; n=10) weeks were not significantly different between ipsilateral and contralateral hemisphere, respectively. However, a significant increase in [^{18}F]DPA-714 uptake is observed in the tumor-bearing hemisphere as compared to the contralateral site at 7 (SUV 0.31 ± 0.11 vs 0.21 ± 0.07; *$p<0.05$; n=10) and 9 (0.32 ± 0.12 vs 0.21 ± 0.08; *$p<0.05$; n=10) weeks (Fig. 1B). Ipsi-to-contralateral ratios rise over time showing significantly increased ratios at 7 and 9 weeks (Supplementary Fig. S2A). In contrast, ipsilateral-to-CC ratios do not increase significantly, but demonstrate significantly decreased values compared to ipsi-to-contralateral at 9 weeks, indicating increased tracer uptake by invasive cells at the CC. Based on the applied thresholding, [^{18}F]DPA-714 volumes significantly increased over time, reaching parts of the contralateral hemisphere (****$p<0.0001$; n=10; Supplementary Fig S2B). Validation of the *in vivo* imaging findings on brain sections using *in vitro* autoradiography with [^{18}F]DPA-714 and hematoxylin/eosin staining confirms glioma growth over time, with infiltration of the tumor into the contralateral hemisphere, especially along the corpus callosum (Fig. 1C).

Human TSPO as the main source of TSPO expression in P3 infiltrative glioma

In vivo [^{18}F]DPA-714 PET indicates tumor growth with infiltration into the contralateral brain hemisphere and significant differences regarding [^{18}F]DPA-714 uptake or volume over time and between the injected and contralateral hemisphere from 7 weeks on. To investigate tumor development and contribution of different tumor components over time immunohistochemistry was performed. Labelling of tumor cells with an anti-human Nestin antibody shows the presence of human glioma cells in the ipsilateral hemisphere and close to the CC as early as 3 weeks. (Fig. 2, hNestin). The labelling spreads within the ipsilateral site but also via the CC into the contralateral site at 5 weeks and extends in both brain hemispheres, but covers nearly the whole ipsilateral site at 7 and 9 weeks of glioma development. As [^{18}F]DPA-714 uptake reflects general TSPO expression, we employed two different antibodies, recognizing primarily the human or specifically the murine TSPO (hTSPO and mTSPO, respectively). Immunofluorescence images show faint human TSPO signal at 3 weeks which, similar to the Nestin labelling, becomes clearly visible at 5 weeks in the ipsilateral hemisphere and its part of the CC (Fig. 2, hTSPO). Comparable to Nestin and in line with the *in vivo* findings the hTSPO staining propagates within the ipsilateral and via the CC into the contralateral hemisphere at 7 and 9 weeks. In contrast, mTSPO staining is barely visible on the overview scans (Fig. 2, mTSPO). Higher resolution images indicate only limited signal within the tumor core or the infiltrative zone (supplementary Fig. S3). Labelling of glioma-associated microglia/macrophages (GAMs), as a possible source of murine TSPO indicates the presence of CD11b$^+$-GAMs as early as 3 weeks around the injection site as well as in the ipsilateral hemisphere and the corresponding CC (Fig. 2, CD11b). The signal evolves from there into neighboring regions and into the contralateral hemisphere at 5, 7 and 9 weeks, underlining the abundance of CD11b$^+$-GAMs in and around the tumor. Only individual CD11b$^+$ cells are also mTSPO$^+$, whereas the majority lacks TSPO expression (supplementary Fig. S3). Less CD11b$^+$-GAMs are present within the tumor after week 9 (Fig. 2, CD11b).

[^{18}F]DPA-714 detects invasively growing glioma before the clinically established radiotracer [^{18}F]FET

To compare [^{18}F]DPA-714 PET with the clinically established tracer for endothelial amino acid transport [^{18}F]FET, PET images for [^{18}F]FET were acquired in addition to [^{18}F]DPA-714 at 7 and at 9 weeks. As reported above, extended [^{18}F]DPA-714 signal is found in the ipsilateral hemisphere at 7 weeks. In contrast, no significant signal for [^{18}F]FET uptake can be demonstrated in the glioma-bearing as compared to the contralateral hemisphere at this time point (p=0.76; Fig. 3). [^{18}F]FET standardized uptake values were 0.36 ± 0.11 vs 0.36 ± 0.13 (ipsi- versus contralateral, respectively; n=5), with an ipsi-to-contralateral ratio of 1.04 ± 0.11. Comparison of [^{18}F]DPA-714 and [^{18}F]FET uptake at 9 weeks shows an increased [^{18}F]FET uptake in the ipsilateral hemisphere with SUVs of 0.55 and 0.96 as compared to SUVs of 0.45 and 0.64, respectively at the contralateral side (n=2). In contrast to [^{18}F]DPA-714, [^{18}F]FET uptake at 9 weeks is found in a restricted area in the ipsilateral but not in the contralateral site (Fig. 3, week 9).

TSPO-PET and diffusion MRI allow early detection of invasively growing glioma

The results of the longitudinal [^{18}F]DPA-714 PET study demonstrate a significant change in [^{18}F]DPA-714 uptake from 7 weeks after tumor implantation. Based on these results, a second study combining [^{18}F]DPA-714 PET with anatomical T_2w- and diffusion MRI was performed in order to investigate particularly glioma growth between 5 and 9 weeks. [^{18}F]DPA-714 uptake at 5 weeks shows faint PET signal localized around the injection tract (Fig. 4A) with SUVs of 0.20 ± 0.02 and 0.17 ± 0.02 for ipsi- and contralateral VOIs, respectively (n=7). Similar to the first longitudinal study, a significant increase in [^{18}F]DPA-714 uptake in the ipsilateral hemisphere is observed at 7 and 9 weeks (Fig. 4B) with SUVs of 0.27± 0.06 vs 0.18 ± 0.02 (week 7: ipsi- versus contralateral, respectively; **p<0.01; n=7) and 0.30 ± 0.07 vs 0.17 ± 0.02 (week 9: ****p<0.0001; n=7). As observed before, 9 weeks p.i. the [^{18}F]DPA-714 PET signal indicates a massive tumor involving nearly the complete ipsilateral brain hemisphere including infiltration into the contralateral side. SUVs in the tumor-implanted site were significantly increased at 9 ($^{\#\#}$p<0.01) and 7 ($^{\#}$p<0.05) weeks as compared to week 5. The corresponding T_2w anatomical MR images depict the needle tract from tumor cell implantation (Fig. 4A, white arrow),

whereas hyperintense areas corresponding to tumor edema can only be seen 9 weeks p.i.. Precise boundaries of the tumor are especially difficult to define.

Non-Gaussian diffusion parameters such as the ADC_0 and kurtosis, as well as the composite marker S-index, provide information on a different level that is tissue microstructure, while information provided by PET is more functional in nature. Whereas parametric maps of the ADC_0 do not show any significant change in the tumor-bearing hemisphere or elsewhere in the brain, kurtosis and S-index parametric maps indicate increased values in the ipsilateral hemisphere and at the site of the CC (Fig. 5A). Comparison of ipsilateral versus contralateral ADC_0, kurtosis or S-index values demonstrates significantly increased values for ipsilateral kurtosis and S-index, whereas no significant differences have been seen for ADC_0 (Fig. 5B). Ipsilateral kurtosis values are significantly higher as compared to the contralateral site from 5 weeks p.i. (0.79 ± 0.02 vs 0.74 ± 0.02; ***p<0.001, 0.82 ± 0.01 vs 0.76 ± 0.02; ***p<0.001, 0.88 ±0.03 vs 0.76 ± 0.02; ****p<0.0001, at 5, 7 and 9 weeks p.i., respectively). Likewise, the S-index shows a significant ipsilateral increase as compared to the contralateral side at week 9 (48.30 ± 5.30 vs 32.35 ± 4.31; **p<0.01), however no difference between the tumor-implanted and the contralateral side is found at week 5 (34.82 ± 8.24 vs 32.02 ± 7.91) or 7 (40.43 ± 3.97 vs 34.12 ± 3.65). Furthermore, ipsilateral kurtosis and S-index are augmented at 9 as compared to 5 ($^{\#\#\#\#}$p<0.0001 and $^{\#\#}$p<0.01) and 7 weeks ($^{\$\$}$p<0.01, kurtosis only), respectively (Fig. 5B).

Discussion

In this study we investigated the feasibility of [^{18}F]DPA-714 PET in combination with diffusion MRI to follow glioma growth and cell infiltration over time in a human invasively growing glioma model. We could demonstrate that longitudinal TSPO-PET imaging allows to monitor and accurately reflect glioma growth and infiltration. Moreover, DWI and [^{18}F]DPA-714 PET were superior over conventional T_2w MRI or [^{18}F]FET PET in early detection of the tumor and tumor infiltration, respectively.

Autoradiography and immunohistochemistry confirmed the presence of an invasively growing tumor as well as distinct TSPO expression closely reflecting tumor growth and infiltration. Tumor growth will yield in changes of cellular density (to which diffusion MRI is sensitive) and vascularization, thus increasing TSPO receptor density and perfusion. However, previous in vivo displacement studies in glioma models demonstrated TSPO specificity[25,34].

It is well known that high grade gliomas extensively infiltrate into the brain parenchyma. However, glioma cell infiltration is usually not detectable by conventional clinical MRI (T_2w, T_1w MRI, with or without gadolinium)[2]. Recently, several groups suggested the potential of TSPO-PET for glioma imaging[15,25,34]. PET or SPECT imaging targeting the translocator protein is a well-known technique for imaging of neuroinflammation as activated microglia highly express TSPO. The fact that some of the recently developed so-called second generation TSPO radioligands have already been translated and assessed in clinical studies of neurodegenerative diseases[35-37], would therefor facilitate application of TSPO imaging in human gliomas.

TSPO expression in the glioma-bearing brain can be of different origin. Specifically in the orthotopic animal model, due to the surgical intervention, inflammatory TSPO may contribute, although sham-operated animals did not show significant tracer uptake[16,25]. We and others have lately shown that the main source of TSPO expression in gliomas is related to neoplastic cells[15,25]. However, also GAMs contribute to the TSPO signal[16,23]. Although individual $TSPO^+$-GAMs could be detected within and around the tumor, we show predominant TSPO expression by tumor cells in this human invasive glioma model. Interestingly, we also found an abundant number of $TSPO^-$-GAMs specifically at the tumor border.

Depending on the literature, 60-85 % of glioma patients express TSPO at moderate to high level[19,20,26] and TSPO imaging would be of value for those patients. Even though kurtosis and the composite S-index did not monitor glioma infiltration as early as [^{18}F]DPA-714 PET, imaging of infiltration into the contralateral hemisphere is improved as compared to T_2w MRI. Furthermore, kurtosis and even the composite S-index, may be well suited for early tumor detection and to some extent infiltration

(although to a later time point) in patients with TSPO-negative GBM or in medical centers without access to PET scanners.

Recent studies suggest that diffusion kurtosis imaging may be useful for differentiating glioma grades and detecting microstructural changes in gliomas[38,39]. Kurtosis reflects the heterogeneous diffusion environments experienced by water molecules as they encounter barriers, move between compartments, and undergo chemical exchange. Thus, this parameter could be sensitive to microstructural modifications of the cerebral parenchyma induced by invasive tumor cells. However, no studies have been evaluated whether kurtosis detects areas of glioma invasion. In this invasive glioma model, we show for the first time that kurtosis is very sensitive for tumor detection as indicated by its early increase in the tumor-bearing hemisphere. We also demonstrate that the S-index, a new metric diffusion combining all DWI parameters, is promising in detection of invasive glioma. In contrast to current approaches based on fitting of DWI signals, which require iterative calculations using complex equations, the quantification of the S-index based on only 2 key b-values, is direct and easy, making the processing time extremely short and compatible with real-time processing in clinical practice.

The other important finding within this study is the advanced/early detection of the invasively growing glioma using [^{18}F]DPA-714 PET and DWI in comparison to conventional T_2w MRI or the clinical imaging biomarker for assessing glioma extent [^{18}F]FET. This result is in accordance with the findings by Jensen and colleagues on TSPO-SPECT imaging in 3 GBM patients, who observed tumor expansion predominantly in areas of high [^{123}I]CLINDE binding as compared to [^{18}F]FET PET and contrast-enhanced structural MRI[40]. Also the multi-tracer imaging approach from Zinnhardt et al. that compared [^{18}F]DPA-714, [^{18}F]BR-351, and [^{18}F]FET in a murine model of glioma indicated a unique area of [^{18}F]DPA-714 positive glioma tissue, with no [^{18}F]FET uptake[16]. Taking into account the clinical TSPO-SPECT data[40] and results from a preclinical TSPO-PET study using human glioma xenotransplants[26] the authors suggested that the unique tissue areas at the tumor margins are of high interest, as they might be related to sites of glioma infiltration, an aspect supported by the outcome of the present study.

Quantification of TSPO-PET bears some challenges, e.g. the different binding affinity patterns for the second generation TSPO ligands in humans due to a genetic polymorphism in the *tspo* gene[41], the question of a suitable reference region for quantification of TSPO binding, and the impact of the vascular component for TSPO quantification[42]. However, results from the present study as well as the recent preclinical and clinical findings should encourage to further investigate TSPO-PET for glioma imaging, in particular for tumor infiltration, as limitations may be tackled e.g. by accounting for the vascular compartment[43] and including genotyping of patients for clinical TSPO-PET studies.

In conclusion, this study strongly supports the high promise of clinical translation of [^{18}F]DPA-714 PET to improve delineation of infiltrative components or glioma-associated-inflammation as confirmed by kurtosis based diffusion imaging which seems to be complementary to other established molecular imaging markers for gliomas.

Funding

Agence National de la Recherche (ANR-11-INBS-0006), EU Seventh Framework Programme (FP7/2007-2013, HEALTH-F2-2011-278850 (INMiND)).

Acknowledgements

The authors thank Emilie Jaumain and Stephane Demphel for their excellent technical support as well as Raphael Boisgard for scientific discussions during the project. We are grateful to Dr. Makoto Higuchi for kindly providing the rodent specific anti-TSPO antibody NP155 and Dr. Hrvoje Miletic for the P3 cells.

References

1. Omuro A, DeAngelis LM. Glioblastoma and other malignant gliomas: a clinical review. *Jama.* Nov 06 2013;310(17):1842-1850.

2. Claes A, Idema AJ, Wesseling P. Diffuse glioma growth: a guerilla war. *Acta Neuropathol.* Nov 2007;114(5):443-458.

3. Dunn GP, Rinne ML, Wykosky J, et al. Emerging insights into the molecular and cellular basis of glioblastoma. *Genes Dev.* Apr 15 2012;26(8):756-784.

4. Dhermain FG, Hau P, Lanfermann H, Jacobs AH, van den Bent MJ. Advanced MRI and PET imaging for assessment of treatment response in patients with gliomas. *Lancet Neurol.* Sep 2010;9(9):906-920.

5. Le Bihan D, Iima M. Diffusion Magnetic Resonance Imaging: What Water Tells Us about Biological Tissues. *PLoS biology.* Jul 2015;13(7):e1002203.

6. Iima M, Yano K, Kataoka M, et al. Quantitative non-Gaussian diffusion and intravoxel incoherent motion magnetic resonance imaging: differentiation of malignant and benign breast lesions. *Investigative radiology.* Apr 2015;50(4):205-211.

7. Iima M, Reynaud O, Tsurugizawa T, et al. Characterization of glioma microcirculation and tissue features using intravoxel incoherent motion magnetic resonance imaging in a rat brain model. *Investigative radiology.* Jul 2014;49(7):485-490.

8. Maximov II, Tonoyan AS, Pronin IN. Differentiation of glioma malignancy grade using diffusion MRI. *Physica Medica.* 2017/07/13/ 2017.

9. Galbán S, Lemasson B, Williams TM, et al. DW-MRI as a Biomarker to Compare Therapeutic Outcomes in Radiotherapy Regimens Incorporating Temozolomide or Gemcitabine in Glioblastoma. *PLOS ONE.* 2012;7(4):e35857.

10. Schmainda KM. Diffusion-weighted MRI as a biomarker for treatment response in glioma. *CNS oncology.* Nov 2012;1(2):169-180.

11. Price SJ, Jena R, Burnet NG, et al. Improved delineation of glioma margins and regions of infiltration with the use of diffusion tensor imaging: an image-guided biopsy study. *AJNR. American journal of neuroradiology.* Oct 2006;27(9):1969-1974.

12. Lutz K, Wiestler B, Graf M, et al. Infiltrative patterns of glioblastoma: Identification of tumor progress using apparent diffusion coefficient histograms. *Journal of magnetic resonance imaging : JMRI.* May 2014;39(5):1096-1103.

13. Iima M, Le Bihan D. Clinical Intravoxel Incoherent Motion and Diffusion MR Imaging: Past, Present, and Future. *Radiology.* Jan 2016;278(1):13-32.

14. la Fougere C, Suchorska B, Bartenstein P, Kreth FW, Tonn JC. Molecular imaging of gliomas with PET: opportunities and limitations. *Neuro Oncol.* Aug 2011;13(8):806-819.

15. Roncaroli F, Su Z, Herholz K, Gerhard A, Turkheimer FE. TSPO expression in brain tumours: is TSPO a target for brain tumour imaging? *Clinical and translational imaging.* 2016;4:145-156.

16. Zinnhardt B, Pigeon H, Theze B, et al. Combined PET imaging of the inflammatory tumor microenvironment identifies margins of unique radiotracer uptake. *Cancer Res.* Jan 30 2017.

17. Black KL, Ikezaki K, Santori E, Becker DP, Vinters HV. Specific high-affinity binding of peripheral benzodiazepine receptor ligands to brain tumors in rat and man. *Cancer.* Jan 1 1990;65(1):93-97.

18. Cornu P, Benavides J, Scatton B, Hauw JJ, Philippon J. Increase in omega 3 (peripheral-type benzodiazepine) binding site densities in different types of human brain tumours. A quantitative autoradiography study. *Acta Neurochir (Wien).* 1992;119(1-4):146-152.

19. Miettinen H, Kononen J, Haapasalo H, et al. Expression of peripheral-type benzodiazepine receptor and diazepam binding inhibitor in human astrocytomas: relationship to cell proliferation. *Cancer Res.* Jun 15 1995;55(12):2691-2695.

20. Vlodavsky E, Soustiel JF. Immunohistochemical expression of peripheral benzodiazepine receptors in human astrocytomas and its correlation with grade of malignancy, proliferation, apoptosis and survival. *J Neurooncol.* Jan 2007;81(1):1-7.

21. Rechichi M, Salvetti A, Chelli B, et al. TSPO over-expression increases motility, transmigration and proliferation properties of C6 rat glioma cells. *Biochim Biophys Acta.* Feb 2008;1782(2):118-125.

22. Veenman L, Levin E, Weisinger G, et al. Peripheral-type benzodiazepine receptor density and in vitro tumorigenicity of glioma cell lines. *Biochem Pharmacol.* Aug 15 2004;68(4):689-698.

23. Awde AR, Boisgard R, Theze B, et al. The Translocator Protein Radioligand 18F-DPA-714 Monitors Antitumor Effect of Erufosine in a Rat 9L Intracranial Glioma Model. *J Nucl Med.* Dec 2013;54(12):2125-2131.

24. Tang D, Hight MR, McKinley ET, et al. Quantitative preclinical imaging of TSPO expression in glioma using N,N-diethyl-2-(2-(4-(2-18F-fluoroethoxy)phenyl)-5,7-dimethylpyrazolo[1,5-a]pyrimi din-3-yl)acetamide. *J Nucl Med.* Feb 2012;53(2):287-294.

25. Winkeler A, Boisgard R, Awde AR, et al. The translocator protein ligand [18F]DPA-714 images glioma and activated microglia in vivo. *Eur J Nucl Med Mol Imaging.* May 2012;39(5):811-823.

26. Buck JR, McKinley ET, Fu A, et al. Preclinical TSPO Ligand PET to Visualize Human Glioma Xenotransplants: A Preliminary Study. *PLoS One.* 2015;10(10):e0141659.

27. Langen K-J, Galldiks N, Hattingen E, Shah NJ. Advances in neuro-oncology imaging. *Nature Reviews Neurology.* 04/07/online 2017;13:279.

28. Keunen O, Johansson M, Oudin A, et al. Anti-VEGF treatment reduces blood supply and increases tumor cell invasion in glioblastoma. *Proc Natl Acad Sci U S A.* Mar 1 2011;108(9):3749-3754.

29. Damont A, Hinnen F, Kuhnast B, et al. Radiosynthesis of [F-18]DPA-714, a selective radioligand for imaging the translocator protein (18 kDa) with PET. *Journal of Labelled Compounds & Radiopharmaceuticals.* Jun-Jul 2008;51(7-8):286-292.

30. Bourdier T, Greguric I, Roselt P, Jackson T, Faragalla J, Katsifis A. Fully automated one-pot radiosynthesis of O-(2-[18F]fluoroethyl)-L-tyrosine on the TracerLab FX(FN) module. *Nucl Med Biol.* Jul 2011;38(5):645-651.

31. Peres EA, Etienne O, Grigis A, Boumezbeur F, Boussin FD, Le Bihan D. Longitudinal Study of Irradiation-Induced Brain Microstructural Alterations With S-Index, a Diffusion MRI Biomarker, and MR Spectroscopy. *Int J Radiat Oncol Biol Phys.* Feb 2 2018.

32. Vollmar SCJ, Sue M, Klein J, Jacobs AH, Herholz K. VINCI-Volume Imaging in Neurological Research, Co-Registration and ROIs Forschung und wissenschaftliches Rechnen 2003. *Göttingen: Gesellschaft für wissenschaftliche Datenverarbeitung.* 2004:115--131.

33. Pottier G, Gomez-Vallejo V, Padro D, et al. PET imaging of cannabinoid type 2 receptors with [11C]A-836339 did not evidence changes following neuroinflammation in rats. *J Cereb Blood Flow Metab.* Mar 2017;37(3):1163-1178.

34. Buck JR, McKinley ET, Hight MR, et al. Quantitative, preclinical PET of translocator protein expression in glioma using 18F-N-fluoroacetyl-N-(2,5-dimethoxybenzyl)-2-phenoxyaniline. *J Nucl Med.* Jan 2011;52(1):107-114.

35. Hamelin L, Lagarde J, Dorothee G, et al. Early and protective microglial activation in Alzheimer's disease: a prospective study using 18F-DPA-714 PET imaging. *Brain : a journal of neurology.* Apr 2016;139(Pt 4):1252-1264.

36. Kreisl WC, Lyoo CH, Liow JS, et al. (11)C-PBR28 binding to translocator protein increases with progression of Alzheimer's disease. *Neurobiology of aging.* Aug 2016;44:53-61.

37. Dupont A-C, Largeau B, Santiago Ribeiro M, Guilloteau D, Tronel C, Arlicot N. Translocator Protein-18 kDa (TSPO) Positron Emission Tomography (PET) Imaging and Its Clinical Impact in Neurodegenerative Diseases. *International journal of molecular sciences.* 2017;18(4):785.

38. Li F, Shi W, Wang D, et al. Evaluation of histopathological changes in the microstructure at the center and periphery of glioma tumors using diffusional kurtosis imaging. *Clinical Neurology and Neurosurgery.* 2016/12/01/ 2016;151:120-127.

39. Qi X-X, Shi D-F, Ren S-X, et al. Histogram analysis of diffusion kurtosis imaging derived maps may distinguish between low and high grade gliomas before surgery. *European Radiology.* April 01 2018;28(4):1748-1755.

40. Jensen P, Feng L, Law I, et al. TSPO Imaging in Glioblastoma Multiforme: A Direct Comparison Between 123I-CLINDE SPECT, 18F-FET PET, and Gadolinium-Enhanced MR Imaging. *J Nucl Med.* Sep 2015;56(9):1386-1390.

41. Owen DR, Yeo AJ, Gunn RN, et al. An 18-kDa translocator protein (TSPO) polymorphism explains differences in binding affinity of the PET radioligand PBR28. *J Cereb Blood Flow Metab.* Jan 2012;32(1):1-5.

42. Rizzo G, Veronese M, Tonietto M, Zanotti-Fregonara P, Turkheimer FE, Bertoldo A. Kinetic modeling without accounting for the vascular component impairs the quantification of [(11)C]PBR28 brain PET data. *J Cereb Blood Flow Metab.* Jun 2014;34(6):1060-1069.

43. Veronese M, Reis Marques T, Bloomfield PS, et al. Kinetic modelling of [11C]PBR28 for 18 kDa translocator protein PET data: A validation study of vascular modelling in the brain using XBD173 and tissue analysis. *J Cereb Blood Flow Metab.* Jan 01 2017:271678X17712388.

Figure captions

Figure 1: Longitudinal TSPO-PET imaging, quantification, autoradiography and histology of the human invasively growing P3 glioma model. A Summed [^{18}F]DPA-714 PET images (30-60 min post injection.) at 1, 3, 5, 7 and 9 weeks p.i. within the same animal indicated glioma growth and infiltration into the contralateral brain hemisphere. White lines represent CT skull contours, white and black circles ipsilateral, contralateral and corpus callosum VOIs, respectively. **B** Tukey boxplot of ipsilateral and contralateral SUVs at the different imaging points displays significant differences between ipsi- and contralateral VOIs at 7 and 9 weeks p.i., respectively (*$p<0.05$; n=10; • outlier). **C** Autoradiography and H&E staining of corresponding coronal mouse brain sections showing [^{18}F]DPA-714 binding and tumor growth over time.

Figure 2: Immunohistochemical distribution of human Nestin (hNestin), human TSPO (hTSPO), CD11b and mouse TSPO (mTSPO) in coronal slices of mouse brains at different time points after glioma cell injection. At 3 weeks p.i. hNestin and CD11b staining indicate the presence of human glioma cells and GAMs, respectively in the ipsilateral brain hemisphere and in proximity to the corpus callosum. hTSPO staining reveals the presence of hTSPO^{+} glioma cells from 5 weeks on.(Scale bar: 1000 μm).

Figure 3: Comparison of [^{18}F]DPA-714 and [^{18}F]FET imaging of the human invasively growing P3 glioma model. PET images were performed at 7 and 9 weeks p.i.. Summed [^{18}F]DPA-714 and [^{18}F]FET PET images (30-60 min p.i.) of the same tumor-bearing animals demonstrate early tumor detection at 7 weeks using [^{18}F]DPA-714 but not [^{18}F]FET. [^{18}F]FET uptake was only detected in a restricted area at

9 weeks p.i.. Ipsi-to-contralateral uptake ratios were significantly higher for [^{18}F]DPA-714 as compared to [^{18}F]FET (****p<0.0001).

Figure 4: C**o-registration of TSPO-PET signal with anatomical T_2w MRI. A** (Left) Summed [^{18}F]DPA-714 PET images (30-60 min p.i.) at 5, 7 and 9 weeks of tumor development. (Middle) Anatomical T_2w images. The white arrow indicates the needle tract from tumor cell implantation. (Right) Fused [^{18}F]DPA-714 PET/T_2w MRI images. **B** Quantification of SUVs of ipsilateral and contralateral VOIs at the different imaging points. [^{18}F]DPA-714 uptake increase in the ipsilateral compared to the contralateral hemisphere is observed at 7 and 9 weeks p.i. (**week 7: p<0.01; n=7 and ****week 9: p<0.0001; n=7) and even in the ipsilateral hemisphere over time ($^{\#\#}$week 9 vs 5: p<0.01 and $^{\#}$week 7 vs 5: p<0.05).

Figure 5: Longitudinal DWI in brain of mice bearing infiltrative glioma. A ADC_0, kurtosis, and S-index mapping determined by a non-Gaussian diffusion model on echo-planar imaging at different points. **B** Comparison of ipsilateral versus contralateral ADC_0, kurtosis or S-index values at 5, 7 and 9 weeks. Significantly increased ipsilateral kurtosis (5, 7, and 9 weeks) and S-index (9 weeks) are observed as compared to contralateral values (**p<0.01, ***p<0.001 and ****p<0.001), whereas no significant differences were observed for ADC_0. Considering the ipsilateral region only, S-index and kurtosis are also significantly higher at 9 as compared to 5 ($^{\#\#}$p<0.01 and $^{\#\#\#\#}$p<0.0001) and 7 weeks of tumor growth ($^{\$\$}$p<0.01, kurtosis only).

Figure 1

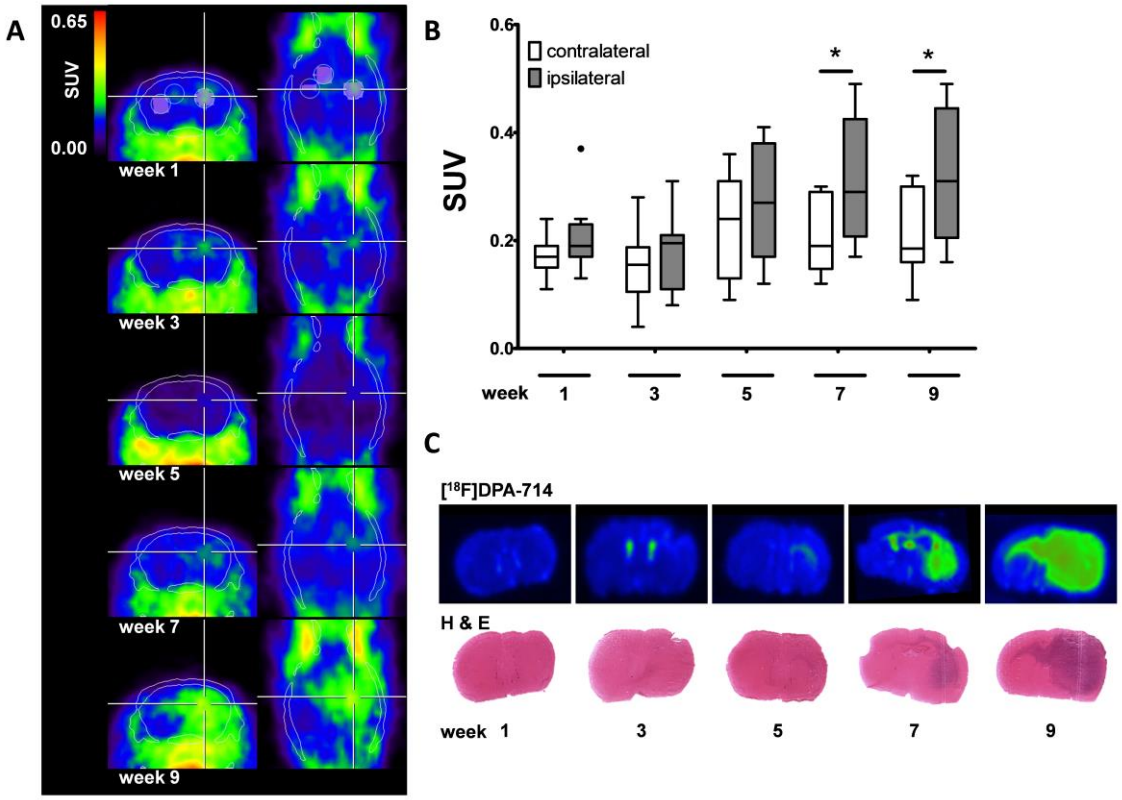
A
0.65
SUV
0.00
week 1
week 3
week 5
week 7
week 9
B
0.6
0.4
0.2
0.0
SUV
contralateral
ipsilateral
*
*
week 1 3 5 7 9
C
[18F]DPA-714
H & E
week 1 3 5 7 9

Figure 2

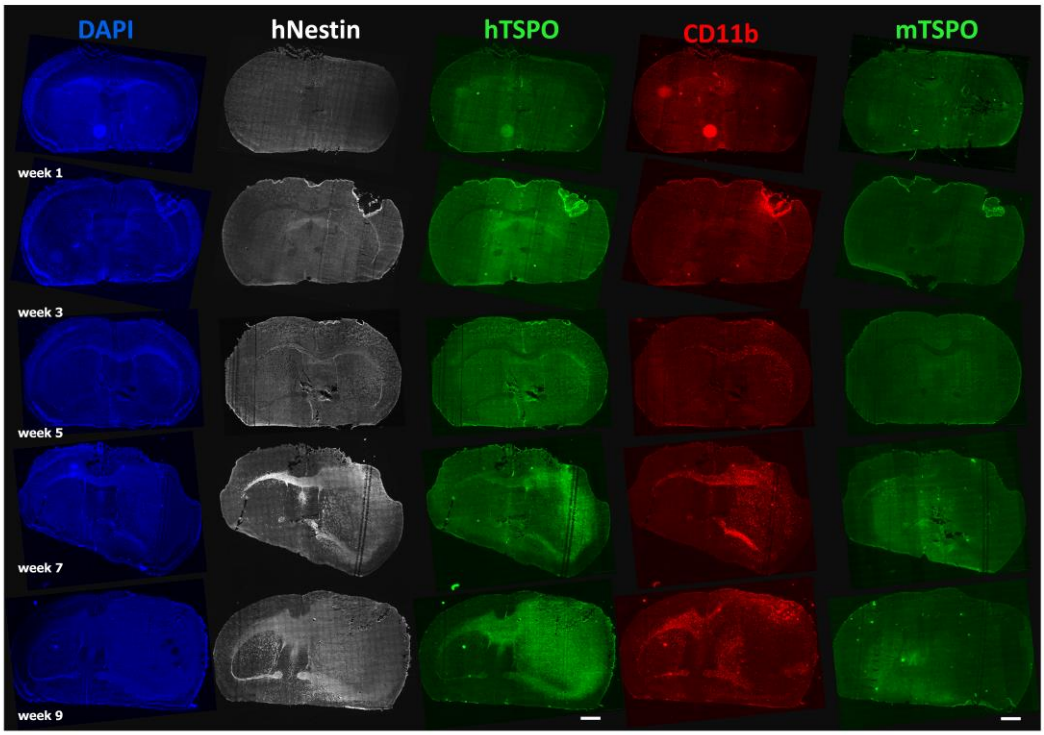
DAPI
hNestin
hTSPO
CD11b
mTSPO
week 1
week 3
week 5
week 7
week 9

Figure 3

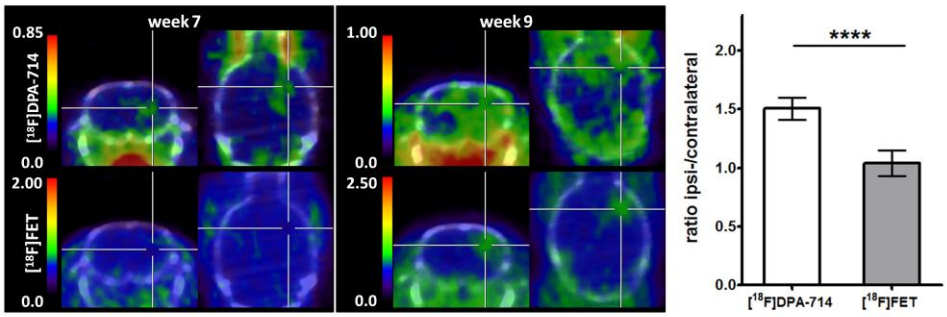
week 7
week 9
0.85
[18F]DPA-714
0.0
2.00
[18F]FET
0.0
1.00
0.0
2.50
0.0
****
ratio ipsi-/contralateral
2.0
1.5
1.0
0.5
0.0
[18F]DPA-714
[18F]FET

Figure 4

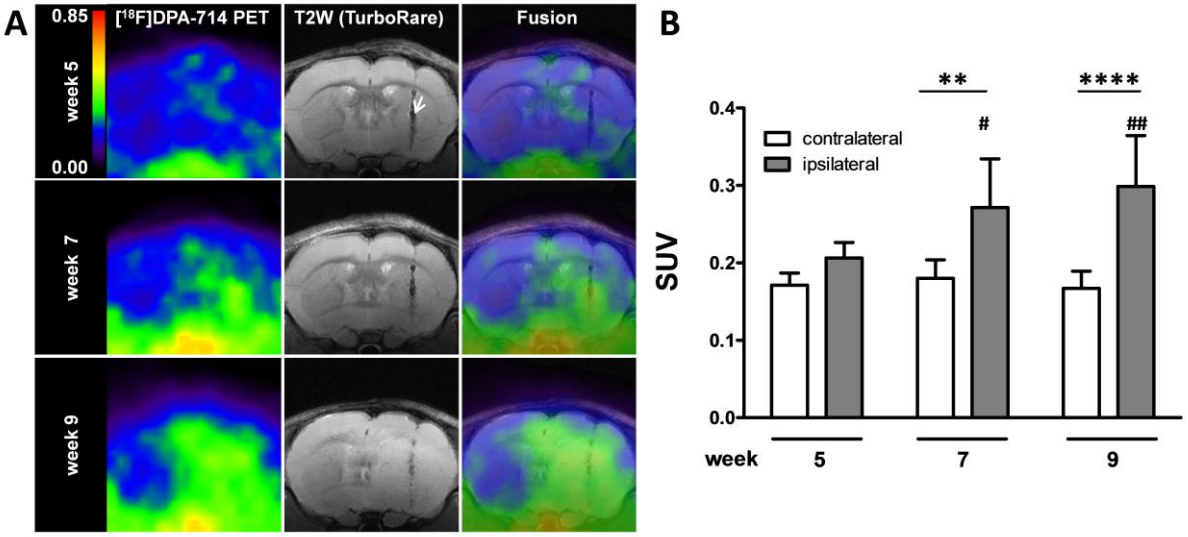
A
0.85
0.00
[18F]DPA-714 PET
T2W (TurboRare)
Fusion
week 5
week 7
week 9
B
SUV
0.4
0.3
0.2
0.1
0.0
contralateral
ipsilateral
**
****
#
##
week
5
7
9

Figure 5

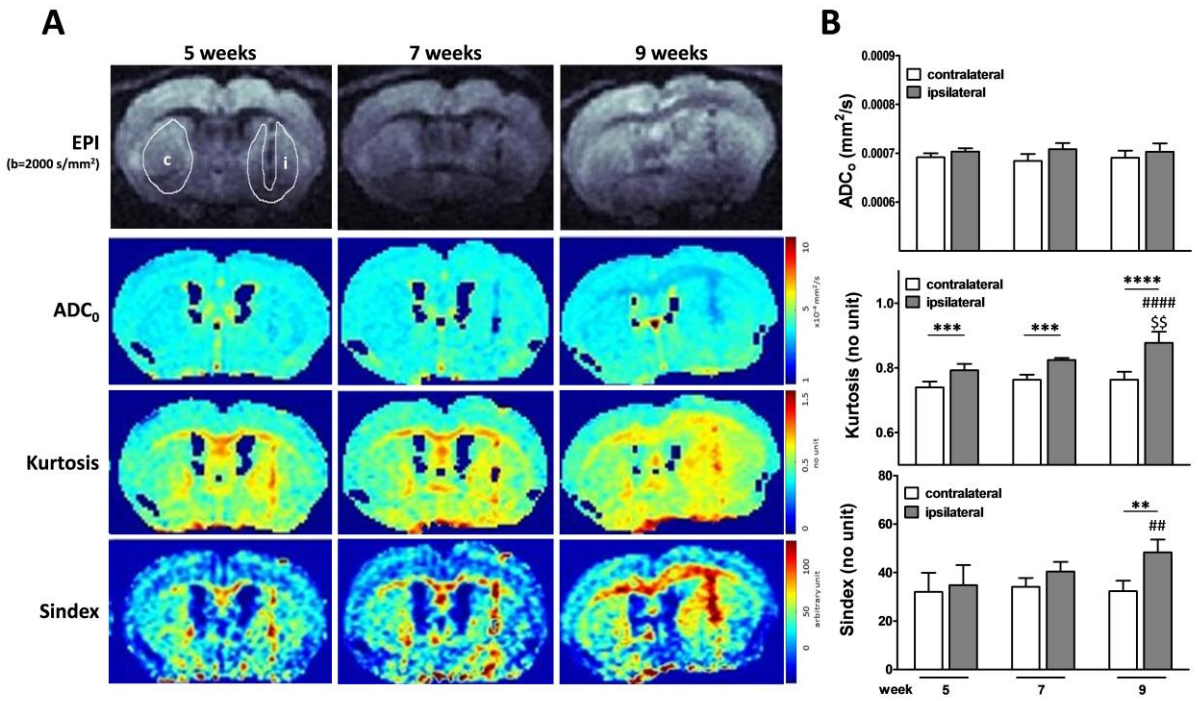
A
5 weeks
7 weeks
9 weeks
EPI
(b=2000 s/mm²)
c
i
ADC0
Kurtosis
Sindex
B
contralateral
ipsilateral
ADC0 (mm²/s)
0.0009
0.0008
0.0007
0.0006
Kurtosis (no unit)
1.0
0.8
0.6
***
***
****
####
$$
Sindex (no unit)
80
60
40
20
0
**
##
week
5
7
9

Supplementary data

Immunohistochemistry

Slides were fixed in 4% paraformaldehyde 15 min at room temperature (RT) and permeabilized using methanol-acetone at a 1:1 volume ratio (-20°C, 5 min) followed by Triton 0.1% in PBS for 5 min at RT. Tissue sections were blocked with 5% bovine serum albumin (BSA, Sigma) in PBS, Tween 0.5% for 15 min at RT, followed by incubation for 1 hour at RT in a humidified chamber with primary antibodies (Supplementary table) in PBS, Tween 0.5%, and BSA 5%. Sections were washed (3 × 5 minutes) in PBS and incubated for 30 min at RT with fluorochrome-conjugated secondary antibodies (Supplementary table) in PBS solution as described above washed again (3 × 5 minutes) in PBS, and mounted with ProLong gold antifade reagent containing 4',6-diamidino-2-phenylindole (DAPI, Invitrogen). Slides were imaged using an AxioObserver Z1 microscope (Zeiss).

PET thresholding approach

Image data were analyzed using VINCI (Version: 4.63.0). We applied a threshold value by multiplying the standard deviation of the control VOI by a factor of 2.5, and adding the resulting counts to the mean value of the control region. This value was used as minimal threshold level within the brain and volumes were calculated. In order to define brain contours, [^{18}F]DPA-714 PET images were manually co-registered to an MRI of a template nude mouse.

MRI acquisitions

The anatomical T_2w MRI was acquired using a Turbo spin-echo sequence (TE/TR = 30/2500 ms, Turbo factor = 8, 2 averages, 16 slices, resolution = 50x50x450 µm). Diffusion-weighted images were acquired using a pulsed-gradient spin-echo echo-planar-imaging sequence (PGSE-EPI, 4 segments, TE/TR=24/2500ms, 16 slices, resolution=125x125x450 µm, δ/Δ=4/11.5ms, 34 b-values from 10 to 3500 s/mm^2, 3 orthogonal directions). µMRI studies were conducted for identification of glioma location,

co-registration to µPET images and evaluated the MRI sensitivity for early detection of infiltrative glioma.

DWI data analysis

In selected regions-of-interest (ROI), the diffusion-weighted signal S(b) was modeled according to the IVIM/non Gaussian (Kurtosis) diffusion model[1]:

$S(b) = S_0 \{f_{IVIM} \exp(-bD^*) + (1-f_{IVIM}) \exp [-bADC_0 + (bADC_0)^2 K/6]\}$

where S_0 is the signal for b=0; f_{IVIM} the volume fraction of incoherently flowing blood in the tissue; *D** the pseudo-diffusion coefficient associated with the IVIM (blood microcirculation) effect; and ADC_0 the virtual ADC for b=0. The Kurtosis (K) is dimensionless coefficient characterizing the heterogeneity of the diffusion process which manifests by a deviation of the diffusion-weighted signal S(b) from a monoexponential decay (K=0 if the probability function of the Brownian motion obeys a Gaussian law). IVIM effects were taken into account to model the overall signals with accuracy, but perfusion parameters were not considered independently. Additionally, *S-index* maps were calculated[2]. *S-index* is a normalized distance (centered at 30 for a "neutral" tissue) allowing the identification of tissue types or structural changes. *S-index* is calculated from the differences of the diffusion-weighted signal S(b) at two or more key b values (b= 200 and 2250 s/mm^2) and simulated signal profiles of signals of 2 reference tissues: a normal brain tissue (f_{IVIM}=1%; ADC_0=0.75 10^{-3}mm²/s; K=0.6) and the tumor tissue with parameters mimicking a cell proliferation (f_{IVIM}=3%; ADC_0=0.65 10^{-3}mm²/s; K=0.8). For each animal, a region-of-interest corresponding to the brain tumor (ipsilateral ROI) was manually delimited in the striatum on three consecutive slices, identified from the presence of tumor cell injection site. In the striatum of the hemisphere opposite to the tumor injection site, a contralateral ROI was delimited on the same slices. Averages values for ADC_0, Kurtosis and *S-index* for each ROI were calculated.

1. Iima M, Yano K, Kataoka M, et al. Quantitative non-Gaussian diffusion and intravoxel incoherent motion magnetic resonance imaging: differentiation of malignant and benign breast lesions. *Investigative radiology.* Apr 2015;50(4):205-211.

2. Iima M, Le Bihan D. Clinical Intravoxel Incoherent Motion and Diffusion MR Imaging: Past, Present, and Future. *Radiology.* Jan 2016;278(1):13-32.

Figure legends

Supplementary Figure S1: Study design for the PET and MRI acquisitions. Study 1 comprises a longitudinal PET study using [^{18}F]DPA-714 to monitor tumor development at week 1, 3, 5, 7, and 9 after tumor implantation as well as a comparison with [^{18}F]FET at week 7. Study 2 combines an multimodal imaging approach using [^{18}F]DPA-714 PET and T_2w and diffusion weighted MRI at week 5, 7 and 9 p.i. In both studies mice were euthanized (†) after the last imaging examination at week 9. Study 3 involves a single [^{18}F]DPA-714 PET examination of n=2 animals at the indicated time point with euthanasia (†) of the animals immediately after the [^{18}F]DPA-714 PET scan. At week 9 an additional [^{18}F]FET PET scan was carried out prior to the [^{18}F]DPA-714 PET. In total 17 animals underwent successfully the complete sequential imaging paradigm, [^{18}F]DPA-714 PET at week 1, 3, 5, 7 and 9 post cell implantation (p.i.; n=10, study 1) or MRI and [^{18}F]DPA-714 PET within 24-48 hours at weeks 5, 7 and 9 p.i. (n=7, study 2)). Additionally, n=10 animals underwent one single [^{18}F]DPA-714 PET acquisition at week 1, 3, 5, 7 or 9 (study 3). Among these animals, n=5 animals also underwent [^{18}F]FET PET 24 hours prior to [^{18}F]DPA-714 PET acquisitions at 7 weeks and n=2 mice at 9 weeks p.i., respectively.

Supplementary Figure S2: Ipsi-to-contralateral or ipsilateral-to-corpus callosum SUV ratios at different imaging points (A) (from 1 to 9 weeks post implantation). A significant increase of ipsi-to-contralateral SUV ratios is observed at 7 and 9 weeks as compared to 1 (**$p<0.01$ and ***$p<0.001$) and 3 weeks (## $p<0.01$) p.i., respectively, indicating a significant increase of tracer uptake in the ipsilateral tumor bearing hemisphere. Ipsilateral-to-corpus-callosum ratios do not increase significantly over time, but demonstrate decreased values compared to ipsi-to-contralateral ratios. A significant decreased ratio is calculated at 9 weeks p.i., indicating increased tracer uptake from invasive

cells at the corpus callosum. **Volumetric analysis of PET tracer uptake over time (B).** Illustration of tracer volumes fused on a T2w MRI template (upper part); [^{18}F]DPA-714 signal volume after thresholding demonstrate significantly increased [^{18}F]DPA-714 volume over time, reaching the contralateral side or parts of the contralateral brain hemisphere (lower part; ****,$^{\#\#\#\#}$p<0.0001; $^{\#\#}$p<0.01; ¤$^{\$}$p<0.05; n=10).

Supplementary Figure S3: Immunohistochemical staining of CD11b and human (hTSPO) or mouse TSPO (mTSPO) in coronal slice of a mouse brain at 9 weeks post glioma cell injection. A Merged overview scan and **B** higher magnification images of hTSPO (green) and CD11b (red) signal in different tumor-related zones as the tumor core (tc), the migratory zone at the corpus callosum (cc) and an infiltrative zone (iz) at the tumor border. **C** Merged overview scan and **D** higher magnification images of mTSPO (green) and CD11b (red) signal in similar zone as described above (tc, cc, iz). (Scale bar: 1000 µm overview scans, 50 µm higher magnification images).

Supplementary figure 1

Supplementary Figure S1

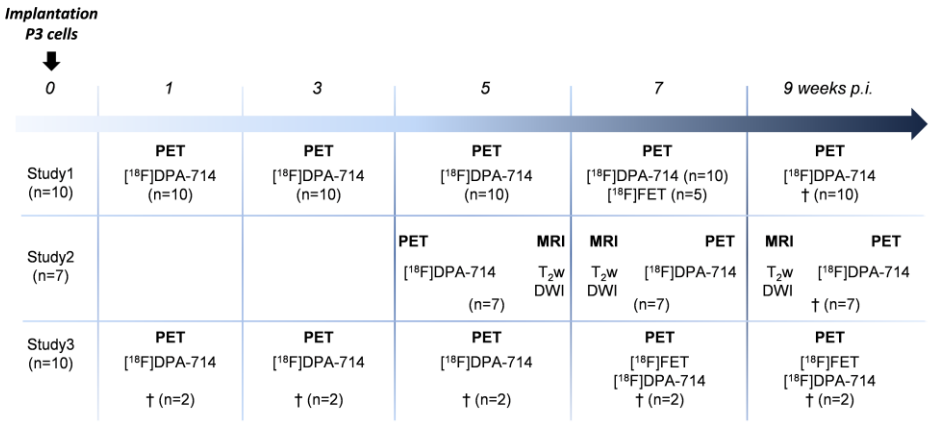

Supplementary figure 2

Supplementary Figure S2

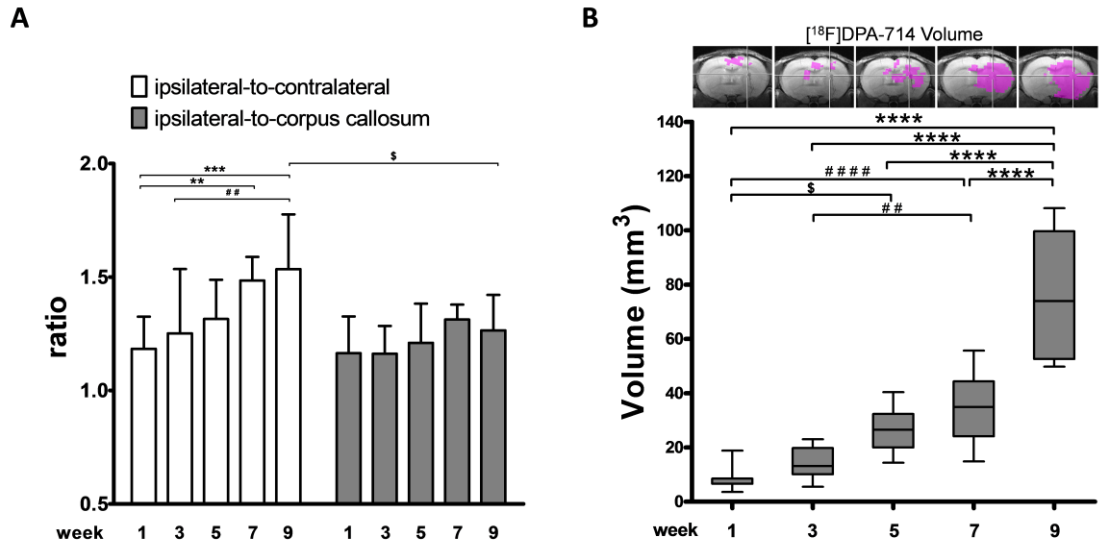

Supplementary figure 3

Supplementary Figure S3